Electronic Supplementary Information (ESI)

Inert nickel doping unlocking aqueous proton storage of hydrated copper hexacyanoferrate as a competitive cathode for proton pseudocapacitors

Jiale Jia, Jizhi Chen, Minyu Jia, Jinfeng Sun,* Linrui Hou, and Changzhou Yuan*

School of Materials Science & Engineering, University of Jinan, Jinan, Shandong 250022, P. R. China

* Corresponding author.

E-mail address: mse_sunjf@ujn.edu.cn (*Prof*. J. Sun)

mse_yuancz@ujn.edu.cn; ayuancz@163.com (*Prof*. C. Yuan).

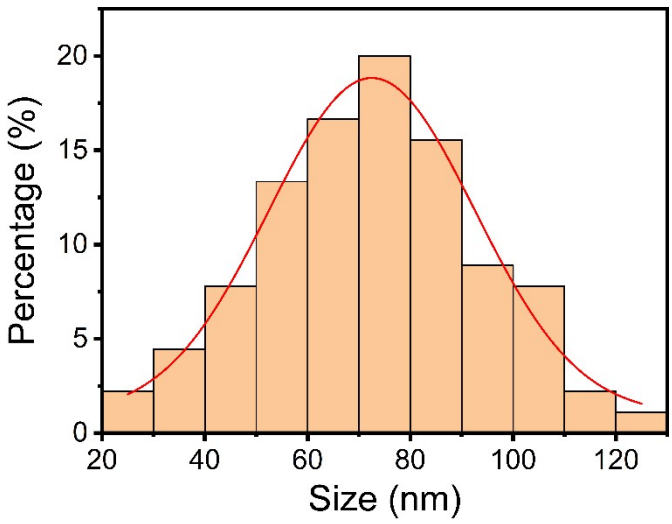

Fig. S1 Particle size distribution diagram of CuHCF-3 obtained from FESEM images.

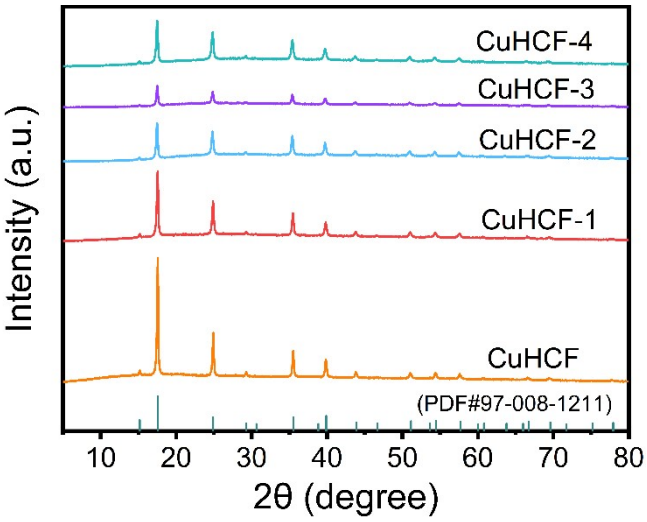

Fig. S2 XRD pattern of CuHCF-X.

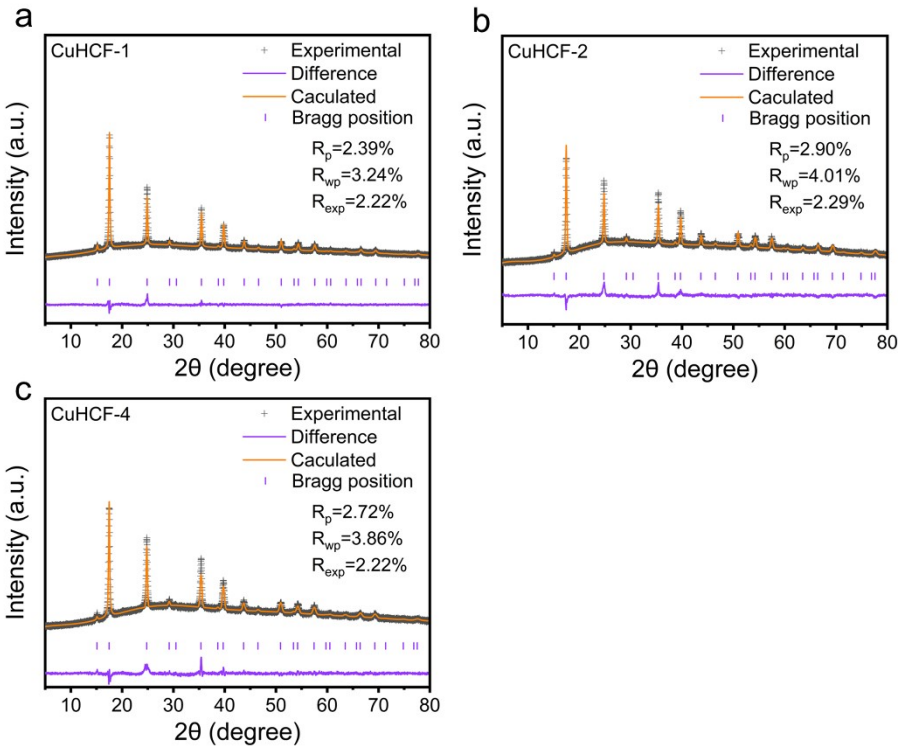

Fig. S3 Rietveld refinements of XRD pattern for (a) CuHCF-1, (b) CuHCF-2, and (c) CuHCF-4.

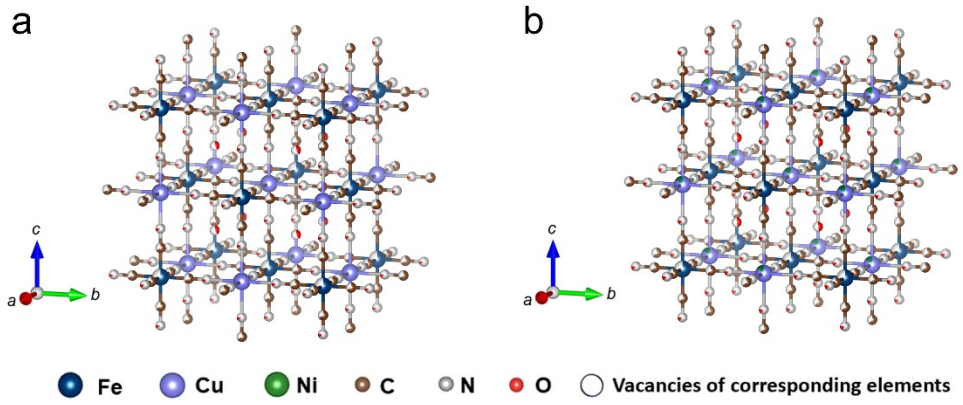

Fig. S4 XRD Rietveld refinement structure for (a) CuHCF and (b) CuHCF-3.

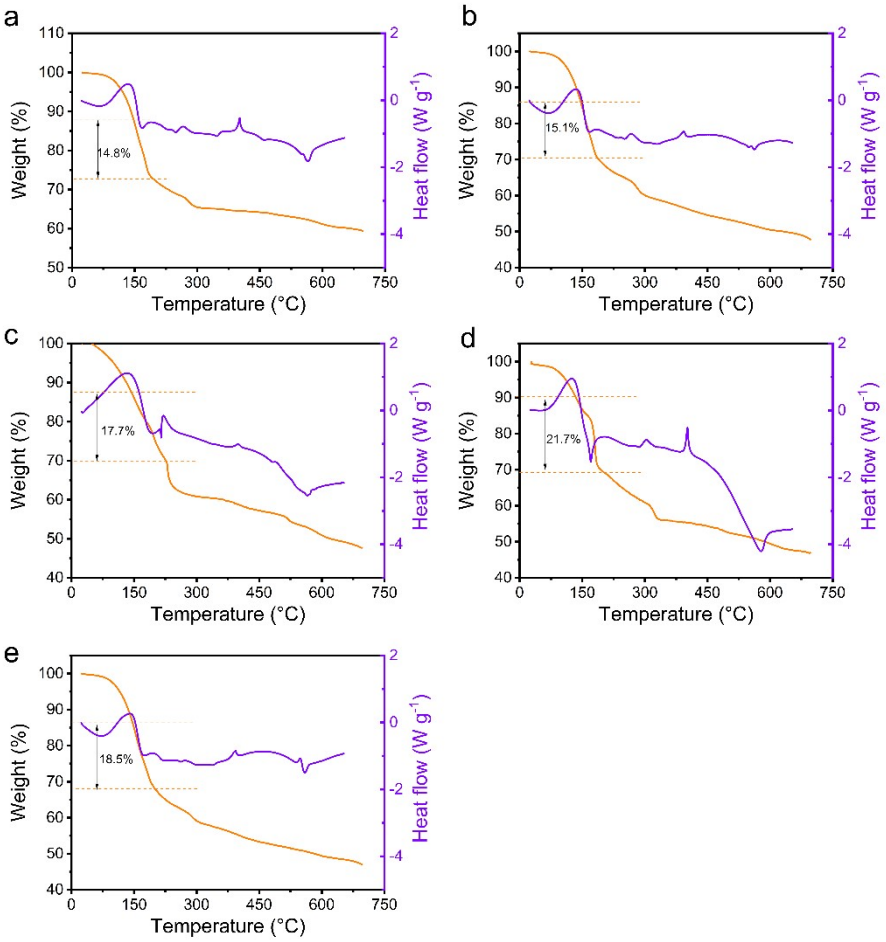

Fig. S5 TG and DSC analysis of (a) CuHCF, (b) CuHCF-1, (c) CuHCF-2, (d) CuHCF-3, and (e) CuHCF-4.

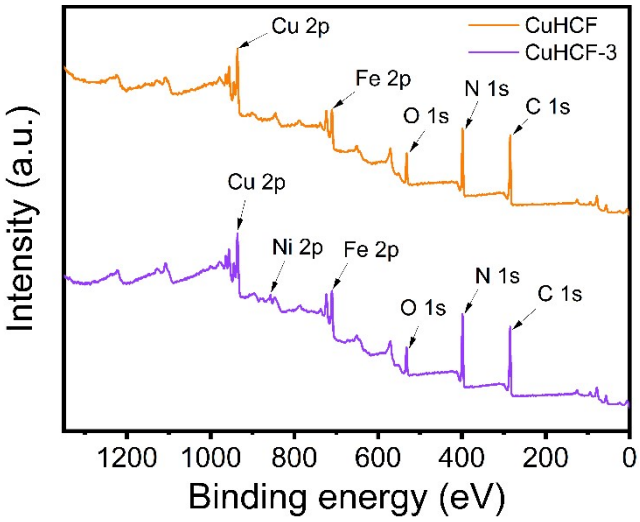

Fig. S6 XPS survey spectra of CuHCF and CuHCF-3.

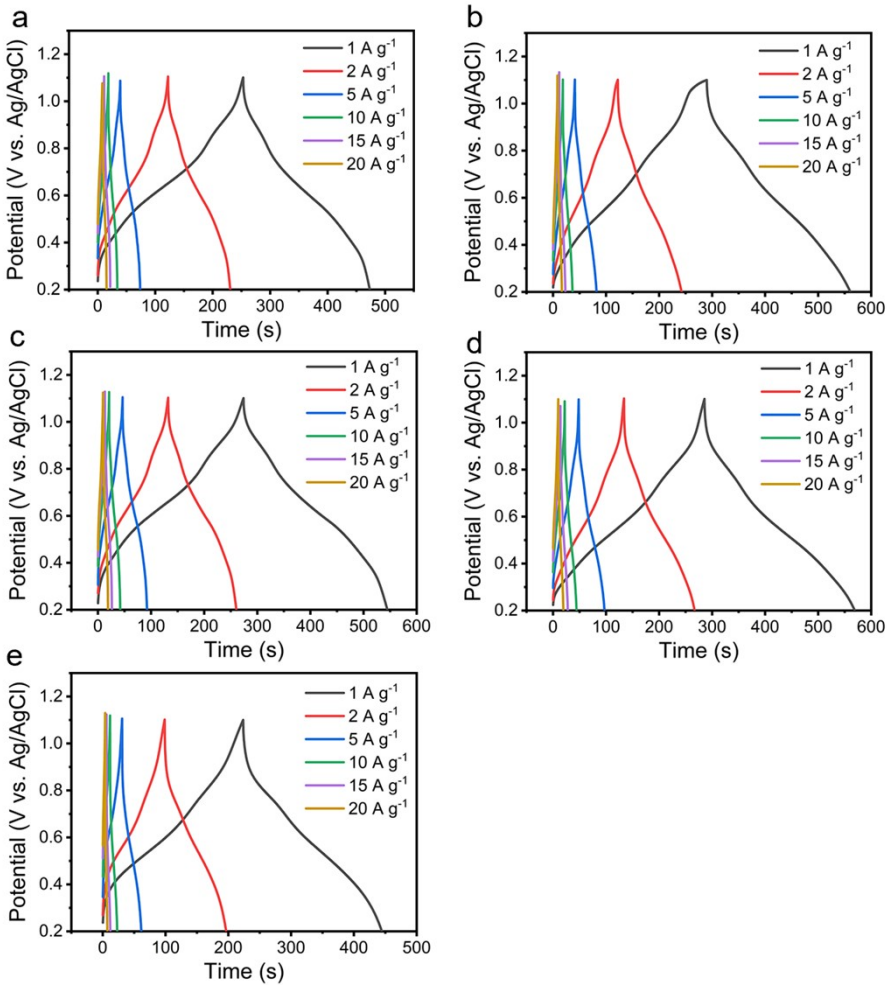

Fig. S7 GCD curves of (a) CuHCF, (b) CuHCF-1, (c) CuHCF-2, (d) CuHCF-3, and (e) CuHCF-4 at different current densities from 1 to 20 A g^{-1}.

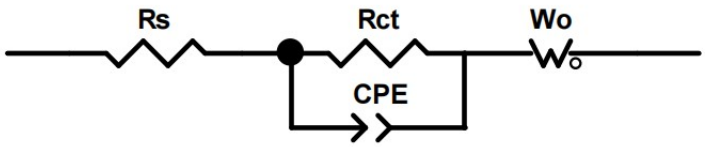

Fig. S8 The equivalent circuit diagram.

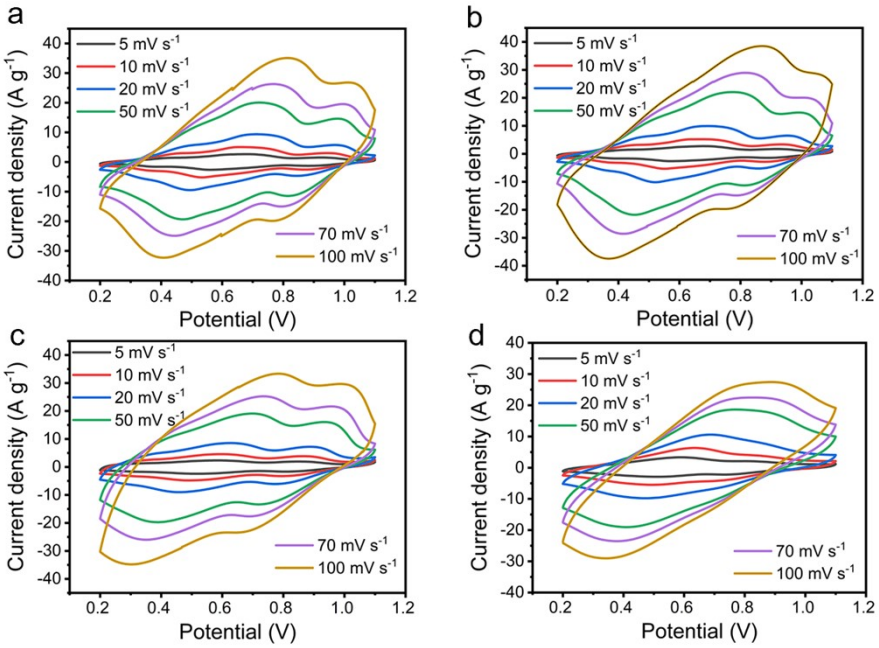

Fig. S9 CV curves of (a) CuHCF, (b) CuHCF-1, (c) CuHCF-2, and (d) CuHCF-4 at different scan rates.

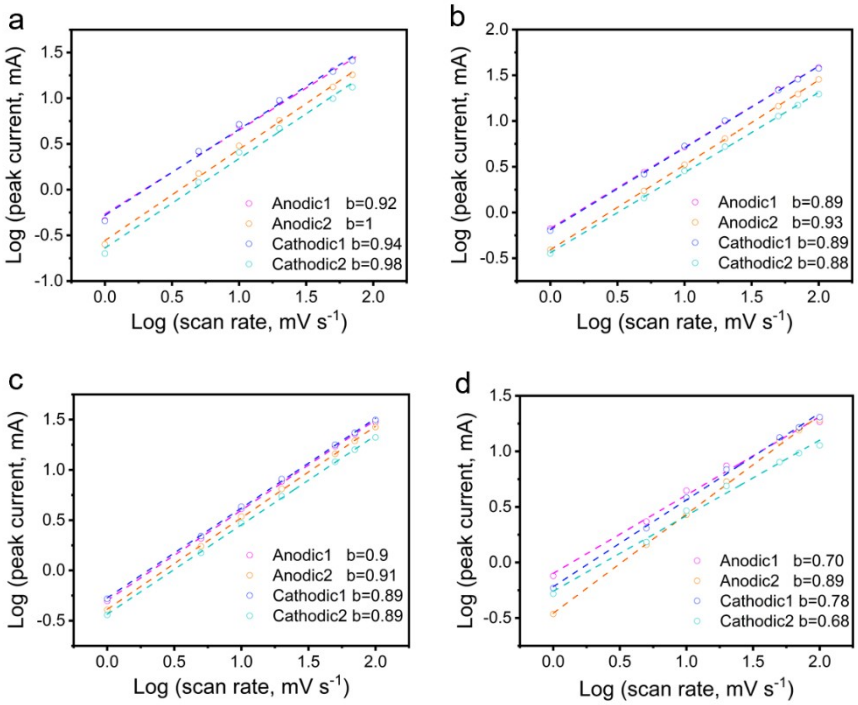

Fig. S10 Relationship between the peak current (*i*) and scan rate (*v*) for (a) CuHCF, (b) CuHCF-1, (c) CuHCF-2, and (d) CuHCF-4.

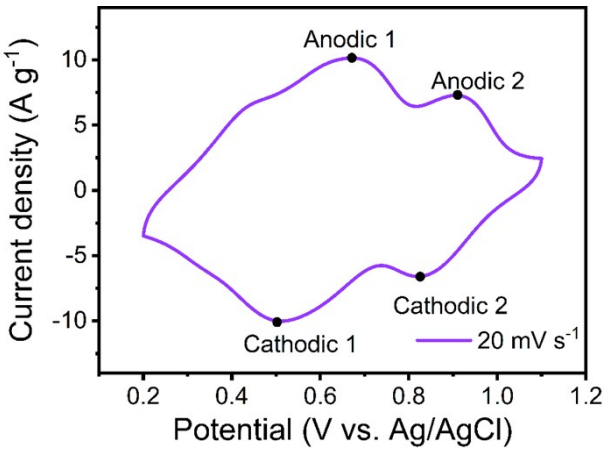

Fig. S11 CV curves of CuHCF-3 at 20 mV s^{-1} and the position of redox peaks.

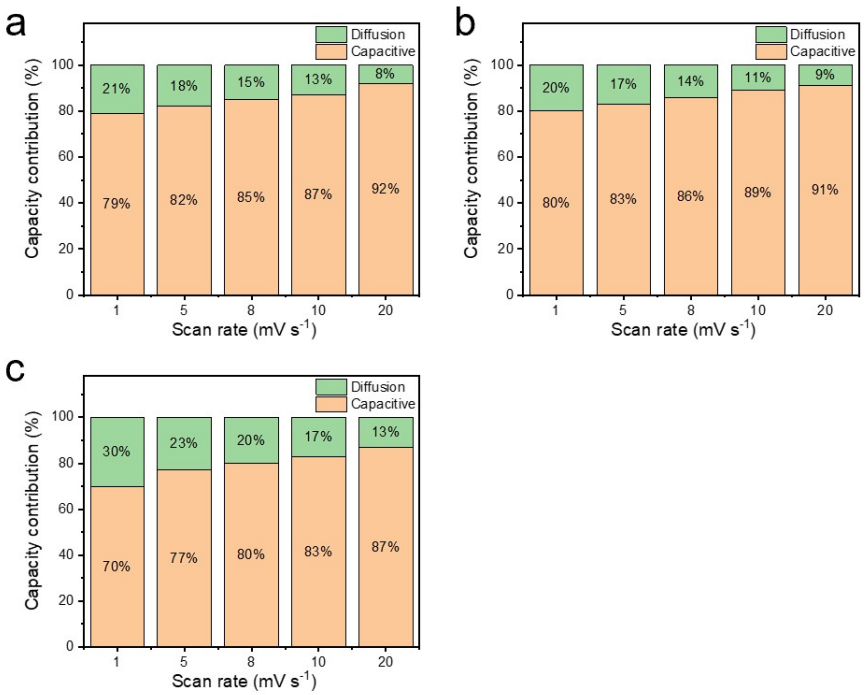

Fig. S12 Capacitive and diffusion contributions at different scan rates for (a) CuHCF-1, (b) CuHCF-2, and (c) CuHCF-4.

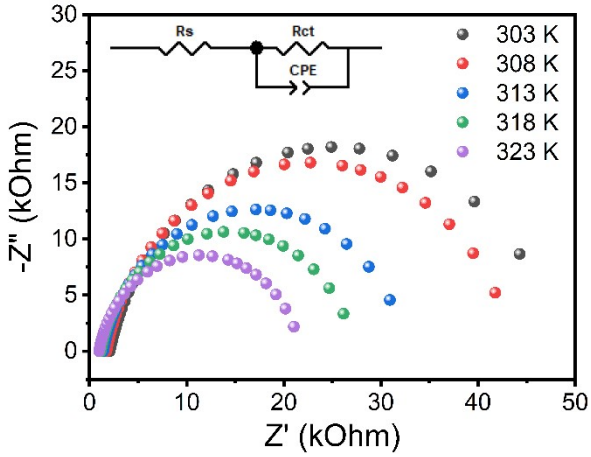

Fig. S13 EIS of CuHCF at different temperatures.

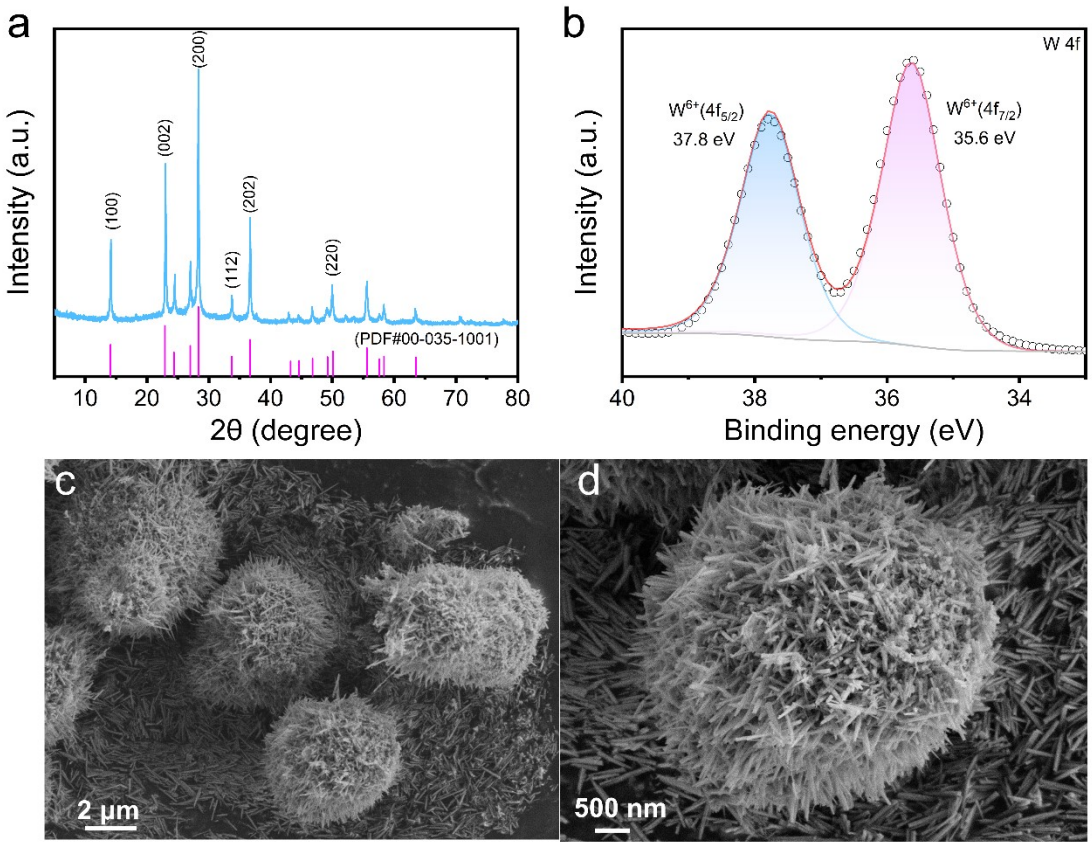

Fig. S14 (a) XRD pattern, (b) high resolution W 4f spectrum, and (c, d) FESEM images of *h*-WO_3.

The high resolution XPS of W 4f indicates that the valence state of W is +6 (Fig. S14b), further verifying the successful synthesis of *h*-WO_3.

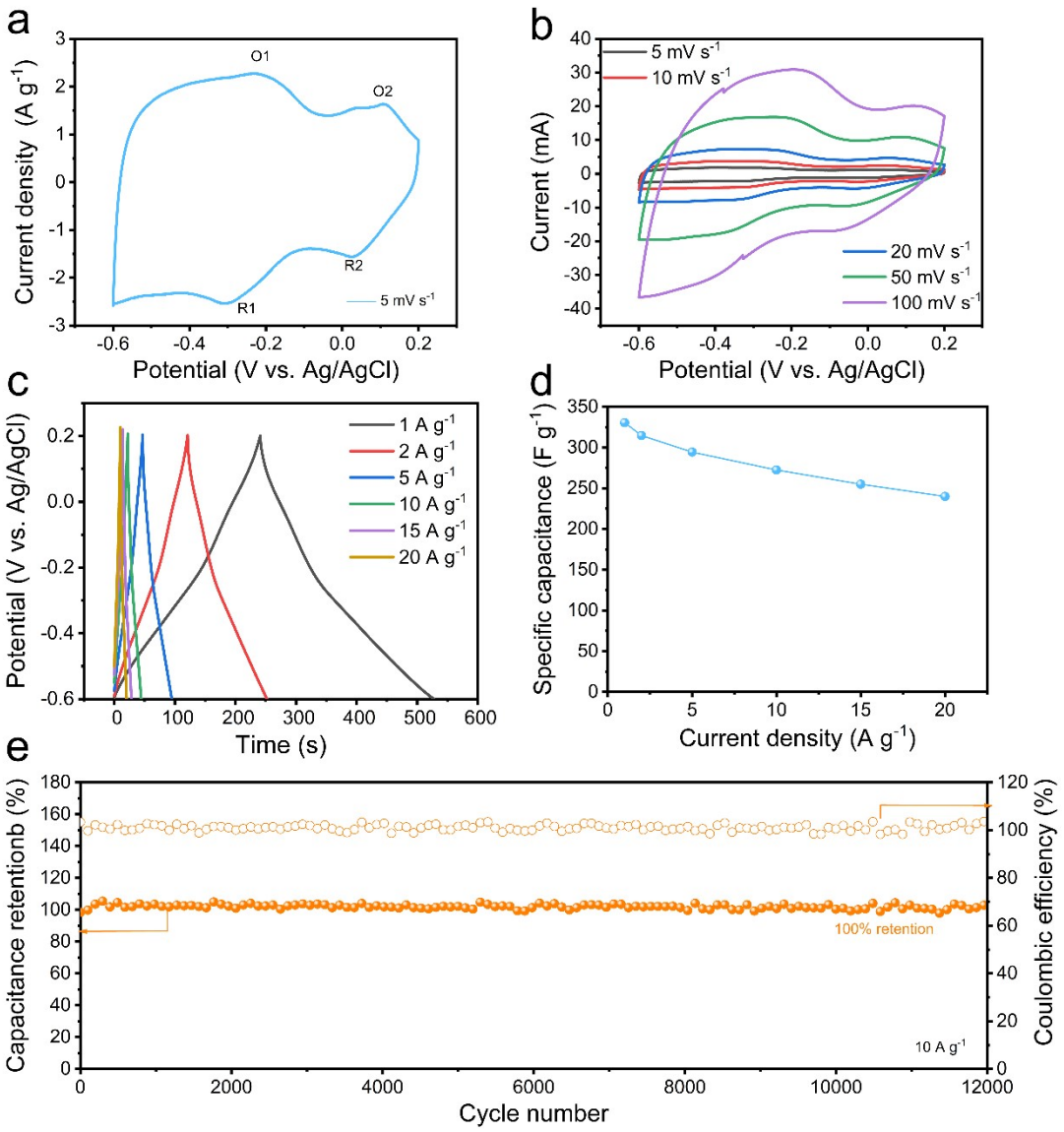

Fig. S15 Electrochemical performance of *h*-WO_3. (a) CV curve at 5 mV s^{-1} along with the marked positions of redox peaks. (b) CV curves at different scan rates. (c) GCD plots and (d) SCs at various current densities**.** (e) Cyclic stability at 10 A g^{-1}.

Table S1 The cell parameters of CuHCF-X with different doping ratios.

Samples	*a* (Å)	*b* (Å)	*c* (Å)
CuHCF	10.109	10.109	10.109
CuHCF-1	10.121	10.121	10.121
CuHCF-2	10.133	10.133	10.133
CuHCF-3	10.142	10.142	10.142
CuHCF-4	10.150	10.150	10.150

Table S2 Structural parameters of CuHCF obtained from Rietveld analysis.

***Fm-3m* space group, a=b=c=10.08 Å, α=β=γ=90°**					
Atom	*x*	*y*	*z*	Occupation	U
Cu	0.50000	0.00000	0.00000	1	0.00633
Fe	0.00000	0.00000	0.00000	0.652	0.00633
C	0.17300	0.00000	0.00000	0.652	0.00633
N	0.28660	0.00000	0.00000	0.652	0.00633
O1	0.28660	0.00000	0.00000	0.102	0.00633
O2	0.25000	0.25000	0.25000	0.396	0.00633

Table S3. Structural parameters of CuHCF-3 obtained from Rietveld analysis.

Fm-3m space group, $a = b = c = 10.14$ Å, $\alpha = \beta = \gamma = 90°$					
Atom	x	y	z	Occupation	U
Cu	0.50000	0.00000	0.00000	0.857	0.01
Ni	0.50000	0.00000	0.00000	0.143	0.01
Fe	0.00000	0.00000	0.00000	0.616	0.00633
C	0.17300	0.00000	0.00000	0.616	0.00633
N	0.28660	0.00000	0.00000	0.616	0.00633
O1	0.28660	0.00000	0.00000	0.140	0.00633
O2	0.25000	0.25000	0.25000	0.463	0.00633

Table S4. ICP-OES analysis results of CuHCF.

Element	Cu	Fe	H_2O
Mass percentage (wt.%)	24.44	13.83	30
Mole ratio	0.38	0.24	1.67

The molar ratio between Cu and Ni was obtained from their mass fractions and atomic masses. The fraction of lattice vacancies (□) is defined as 1−[n(Fe) / (n(Cu) + n(Ni))], where n represents the molar quantity. The hydration number *x* is given by the molar ratio of water molecules to the anhydrous PBA framework.

Table S5 ICP-OES analysis results of CuHCF-3.

Element	Cu	Ni	Fe	H_2O
Mass percentage (wt.%)	20.69	3.17	12.88	31.8
Mole ratio	0.32	0.054	0.23	1.77

Table S6 Comparison for rate performance of CuHCF-3 with reported cathode materials.

Material	Electrolyte	Capacitance/Capacity (Current density)	Rate performance	Retention	Ref.
CNT/NK-COF	2 M H_2SO_4	340 F g^{-1} (1 A g^{-1})	216 F g^{-1} (20 A g^{-1})	~64%	1
PANI/rGO	1 M H_2SO_4	346 F g^{-1} (0.5 A g^{-1})	225 F g^{-1} (10 A g^{-1})	~65%	2
VOHCF	2 M H_2SO_4	67.3 mAh g^{-1} (1 A g^{-1})	39.6 mAh g^{-1} (20 A g^{-1})	~59%	3
MoO_3	7.1 M H_2SO_4	43 mAh g^{-1} (1 A g^{-1})	20 mAh g^{-1} (5 A g^{-1})	~47%	4
VHCF	6 M H_2SO_4	90 mAh g^{-1} (1 A g^{-1})	65 mAh g^{-1} (10 A g^{-1})	~72%	5
InHCF	0.05 M H_2SO_4	52.3 mAh g^{-1} (1 A g^{-1})	33.7 mAh g^{-1} (6 A g^{-1})	~64%	6
NiPBA	4.5 M $H_2C_2O_4$	~50 mAh g^{-1} (0.5 A g^{-1})	~32 mAh g^{-1} (5 A g^{-1})	~64%	7
PAD-COF	1.2 M H_2SO_4	126 mAh g^{-1} (0.2 A g^{-1})	73 mAh g^{-1} (6 A g^{-1})	~58%	8
CuHCF-3	0.5 M H_2SO_4	316 F g^{-1} (1 A g^{-1})	217 F g^{-1} (20 A g^{-1})	69%	This work

Table S7 EIS fitting results of the CuHCF-X cathodes.

Cathodes	CuHCF	CuHCF-1	CuHCF-2	CuHCF-3	CuHCF-4
R_{ct} (Ω)	1.83	1.72	1.64	1.45	1.87
R_s (Ω)	1.79	1.83	1.43	1.40	1.18

Table S8 Bulk impedance at different temperatures of CuHCF and CuHCF-3.

Temperature (K)	303	308	313	318	323
Bulk impedance of CuHCF (Ω)	2069.0	1722.0	1408.2	1153.0	994.8
Bulk impedance of CuHCF-3 (Ω)	1013.0	807.4	686.1	604.4	548.8

Table S9 Proton conductivity comparison of PBA-based materials.

Material	Sample form	Test condition	Proton conductive	Ref.
VCr-PBA	pelletized powder	High-humidity environment	1.6×10^{-3} (293 K)	9
Im-HAc@CuHCC	pelletized powder	98% RH	9.33×10^{-3} (298 K)	10
$Cu_{0.82}Co_{0.18}HCF$	pelletized powder	100% RH	4×10^{-5} (303K)	11
CuHCF	pelletized powder	0% RH	7.43×10^{-8} (293 K)	12
CuHCF-3	pelletized powder	High-humidity environment	5×10^{-5} (303K)	This work

Table S10 Comparison of CuHCF-3 with reported PBA-based and other proton pseudocapacitors.

Cathode//Anode	Power density	Energy density	Current density	Stability (Cycles/Retention)	Ref.
NiFe-PBA//P-MoO_3	64 kW kg^{-1}	17 Wh kg^{-1}	20 A g^{-1}	5000/100%	13
$Cu_{0.82}Co_{0.18}$HCF//*h*-MoO_3	21 kW kg^{-1}	21 Wh kg^{-1}	10 A g^{-1}	10000/83%	14
CuCoHCF//MXene	20 kW kg^{-1}	27 Wh kg^{-1}	20 A g^{-1}	26000/93%	15
VOHCF//HATN	0.35 kW kg^{-1}	41.2 Wh kg^{-1}	1 A g^{-1}	200/87%	3
InHCF//DPPZ	~0.2 kW kg^{-1}	28 Wh kg^{-1}	6 A g^{-1}	3000/76.1%	6
TABQ//TCBQ	2.5 kW kg^{-1}	~7.5 Wh kg^{-1}	5 A g^{-1}	3500/71.2%	16
$W_{18}O_{49}$/$Ti_3C_2T_x$//RuO_2@CC	2 kW kg^{-1}	24.1 Wh kg^{-1}	10 A g^{-1}	4000/81.5%	17
PYT-GN 4-5//A-$Ti_3C_2T_x$	7 kW kg^{-1}	13.2 Wh kg^{-1}	3 A g^{-1}	5000/91.4%	18
MoO_3/$Ti_3C_2T_z$//NAC	37.5 kW kg^{-1}	~10 Wh kg^{-1}	10 A g^{-1}	10000/94.2%	19
PPHZ//MnO_2	4.8 kW kg^{-1}	16.9 Wh kg^{-1}	4 A g^{-1}	30000/94.7%	20
CuHCF-3//*h*-WO_3	20 kW kg^{-1}	25 Wh kg^{-1}	10 A g^{-1}	20000/100%	This work

Reference

1. Y. Yang, P. Zhang, L. Hao, P. Cheng, Y. Chen and Z. Zhang, *Angew. Chem. Int. Ed.*, 2021, **60**, 21838-21845.

2. H. Yu, Y. Long, D. Chen, X. Dong, X. Ye, Y. Zhang, F. Li, Y. Xu, Y. Tao and Q. H. Yang, *Small*, 2024, **20**, e2303832.

3. J. Yang, W. Hou, L. Ye, G. Hou, C. Yan and Y. Zhang, *Small*, 2023, **20**, 2305386.

4. A. Ikezawa, Y. Koyama, T. Nishizawa and H. Arai, *J. Mater. Chem. A*, 2023, **11**, 2360-2366.

5. X. Peng, H. Guo, W. Ren, Z. Su and C. Zhao, *Chem. Commun.*, 2020, **56**, 11803-11806.

6. J. Qiao, M. Qin, Y. M. Shen, J. Cao, Z. Chen and J. Xu, *Chem. Commun.*, 2021, **57**, 4307-4310.

7. B. Gavriel, G. Bergman, M. Turgeman, A. Nimkar, Y. Elias, M. D. Levi, D. Sharon, N. Shpigel and D. Aurbach, *Mater. Today Energy*, 2023, **31**, 101189.

8. X. Yan, F. Wang, X. Su, J. Ren, M. Qi, P. Bao, W. Chen, C. Peng and L. Chen, *Adv. Mater.*, 2023, **35**, 2305037.

9. Y. Hu, Z. Guo, Y. Chen, C. Zhou, Y. C. Li and S. Ren, *Nat. Commun.*, 2022, **13**, 7056.

10. Q. Qiao, H.-J. Wang, C.-P. Li, X.-Z. Wang and X.-M. Ren, *Inorg. Chem. Front.*, 2021, **8**, 2305-2314.

11. T. Xu, Z. Li, D. Wang, M. Zhang, L. Ai, Z. Chen, J. Zhang, X. Zhang and L. Shen, *Adv. Funct. Mater.*, 2021, **32**, 2107720.

12. P. Hosseini, K. Wolkersdörfer, M. Wark, E. Redel, H. Baumgart and G. Wittstock, *J. Phys. Chem. C*, 2020, **124**, 16849-16859.

13. J. Gao, Y. Liu, Y. Zhang, B. Jin, Y. Lu, Y. Wu, S. Zhang, T. Han, J. Guo, H. Yan and M. Shao, *Adv. Funct. Mater.*, 2025, DOI: 10.1002/adfm.202522130.

14. T. Xu, Z. Xu, T. Yao, M. Zhang, D. Chen, X. Zhang and L. Shen, *Nat. Commun.*, 2023, **14**, 8360.

15. Y. Wang, H. Song, Z. Lu, J. Dong, X. Xu, J. Wu, H. Yu and L. Yuan, *Chem. Eng. J.*, 2026, **527**, 172058.

16. S. Wu, M. Taylor, H. Guo, S. Wang, C. Han, J. Vongsvivut, Q. Meyer, Q. Sun, J. Ho and C. Zhao, *Angew. Chem. Int. Ed.*, 2024, **63**, e202412455.

17. Y. Zhang, Q. Jin, L. Li, M. Zhang, J. Wen, L. Wu, H. Gao, X. Zhang and L. Li, *Carbon*, 2023, **208**, 92-101.

18. M. Shi, C. Peng and X. Zhang, *Small*, 2023, **19**, 2301449.

19. W. Zheng, J. Halim, A. El Ghazaly, A. S. Etman, E. N. Tseng, P. O. Å. Persson, J. Rosen and M. W. Barsoum, *Adv. Sci.*, 2021, **8**, 2003656.

20. R. Wang, J. He, C. Yan, R. Jing, Y. Zhao, J. Yang, M. Shi and X. Yan, *Adv. Mater.*, 2024, **36**, 2402681.